

Article

Effect of Molybdenum Coatings on the Accelerating Cavity Quality Factor

Pablo Vidal García ^{1,2,*} , Stefano Sarti ³ , Martina Carillo ^{4,5}, Lucia Giuliano ^{4,5} , Augusto Marcelli ^{6,7} , Bruno Spataro ⁶ , Andrea Alimenti ¹ , Kostiantyn Torokhtii ¹ , Enrico Silva ^{1,2}  and Nicola Pompeo ^{1,2} 

¹ Department of Industrial, Electronic and Mechanical Engineering, Roma Tre University, 00146 Rome, Italy; andrea.alimenti@uniroma3.it (A.A.); kostiantyn.torokhtii@uniroma3.it (K.T.); enrico.silva@uniroma3.it (E.S.); nicola.pompeo@uniroma3.it (N.P.)

² National Institute for Nuclear Physics, Roma Tre Section (INFN-Roma Tre), 00146 Rome, Italy

³ Department of Physics, Sapienza University of Rome, 00185 Rome, Italy; stefano.sarti@uniroma1.it

⁴ SBAI Department, Sapienza University of Rome, 00161 Rome, Italy; martina.carillo@uniroma1.it (M.C.); lucia.giuliano@uniroma1.it (L.G.)

⁵ National Institute for Nuclear Physics, Roma Section (INFN-Roma), 00185 Rome, Italy

⁶ National Institute for Nuclear Physics, Frascati National Laboratory (INFN-LNF), Frascati, 00044 Rome, Italy; augusto.marcelli@lnf.infn.it (A.M.); bruno.spataro@lnf.infn.it (B.S.)

⁷ Rome International Centre for Material Science Superstripes (RICMASS), 00185 Rome, Italy

* Correspondence: pablo.vidalgarcia@uniroma3.it

Abstract: In this work, a detailed parametric study assessing the impact of low-conductivity coatings on the radio-frequency accelerating cavity quality factor and resonance frequency shift is presented. In particular, this study is aimed at proving the feasibility of molybdenum oxides deposited on copper to reduce the dark current in high-gradient applications due to its intrinsically high work function. In order to compute the effective surface impedance of the resulting layered structure, a transmission line-based approach is adopted. The present analysis demonstrates the potential effectiveness of molybdenum thin-films, which only slightly affects the accelerating cavity quality factor, with very low sensitivity to thickness and resistivity inhomogeneities.

Keywords: accelerating cavities; molybdenum coatings; effective surface impedance; dark current; RF breakdown; high brightness accelerators



Citation: Vidal García, P.; Sarti, S.; Carillo, M.; Giuliano, L.; Marcelli, A.; Spataro, B.; Alimenti, A.; Torokhtii, K.; Silva, E.; Pompeo, N. Effect of Molybdenum Coatings on the Accelerating Cavity Quality Factor. *Instruments* **2023**, *7*, 33. <https://doi.org/10.3390/instruments7040033>

Academic Editor: Antonio Ereditato

Received: 30 July 2023

Revised: 16 October 2023

Accepted: 17 October 2023

Published: 21 October 2023



Copyright: © 2023 by the authors. Licensee MDPI, Basel, Switzerland. This article is an open access article distributed under the terms and conditions of the Creative Commons Attribution (CC BY) license (<https://creativecommons.org/licenses/by/4.0/>).

1. Introduction

The accelerating gradient is one of the major limiting factors of cavities in radio frequency (RF) particle accelerators. In large-scale experiments, it definitively determines the cost and thus the viability of linear colliders in high energy physics projects, such as the CERN-based Compact Linear Collider (CLIC) [1], or high brightness electron sources used in free electron lasers (FELs), such as the Linac Coherent Light Source (LCLS) [2]. In room-scale cost-effective setups, light sources benefit from high brightness beams to meet with applications of great interest among the structural dynamics imaging community [3].

The main maximum field intensity limitation is due to the RF vacuum breakdown in copper cavities [4]. Breakdown is pointed to be the origin of irreversible damage on the cavity surface, leading to quality factor (Q_0) degradation [5]. The current interpretation of the beginning of breakdowns points to movements of crystal defects induced by periodic thermo-mechanical stresses (known as pulse heating). Indeed, there is experimental evidence [5,6] supporting the pulse heating hypothesis, based on the operation at cryogenics to reduce the copper thermal expansion coefficient and simultaneously increase the yield strength, and so the material hardness. However, the phenomenon acting as a definitive breakdown trigger has been a fact of discussion for years (see chronologically [5,7]): it is widely accepted that first breakdowns originate from dust particle heating and high field-enhanced factor features favored by surface gas desorption. In those cases, the appropriate

RF conditioning eventually leads to surpass such breakdowns. Beyond that, the breakdowns are not fully understood. Nevertheless, there are accurate analytical estimations [8] preferably in favor of the formation enthalpy of defects when the electric field exceeds the tensile strength of copper causing the breakdown. The corresponding model can explain the breakdown rate (BDR) power law $BDR \propto E_{acc}^{\zeta}$ with $\zeta \approx 30$ seen in experiments [6]. At such high fields ($E_{acc} > 300$ MV/m), and accounting for the field enhancement factor derived from field emitted currents (≈ 30), the binding potential of atoms is exceeded and dark currents can directly melt copper. Consequently, reducing dark currents may be critical to prevent the cavity from breakdowns and avoid the subsequent damage.

In order to reduce the BDR, different strategies have been proposed [9]: on one hand, there is potential in engineering the next generation of high brightness electron sources at higher frequencies so that the time pulse (t_p) is reduced, and thus the pulse heating. On the other hand, the use of non-annealed harder copper alloys (CuAg, CuCr, and CuZr) could mitigate the surface damage caused by breakdowns. With the same purpose, different experiments using hybrid accelerating structures made of copper at the cavity walls and molybdenum at the irises were carried out; first at the CLIC Test Facility [10] resulting in an appreciable improvement on the maximum achievable E_{acc} before the breakdown; and then at the Stanford Linear Accelerator Centre (SLAC) [11] with no clear advantages with respect to the same structures made of copper. Despite these attempts, so far the issues related to the intrinsic relative work function of copper and its role in triggering breakdowns are not demonstrated. Nevertheless, it was proved [12] that dark current beam loading plays a fundamental role in describing the Q_0 degradation observed when pulsing the cavity for a constant accelerating field (E_{acc}). Having this in mind, a straightforward path to reduce the Fowler–Nordheim currents [13] consists in growing coatings characterized by augmented local work function (WF), which may hint at the final cause of breakdowns. This constitutes the main motivation of the previous works [14,15] pursuing the implementation of those coatings in high-gradient accelerating structures.

Among Transition Metal Oxides (TMO), molybdenum trioxide MoO_3 , in the form of thin-films grown at room temperature by solid phase deposition on polycrystalline Cu, exhibits interesting properties for coating accelerating structures [16]: (i) they exhibit an amorphous orthorhombic phase (α - MoO_3), characterized by a noticeably augmented and relatively invariant WF (ϕ_{MoO_3}) with respect to copper (ϕ_{Cu}): $\phi_{MoO_3} - \phi_{Cu} = (1.8 \pm 0.5)$ eV in 100 nm of MoO_3 coating on copper; (ii) the transport properties may be finely tuned by varying the film thickness. While coating layers of (30 to 300) nm show metallic behavior, thicker films behave as semiconductors. For accelerating cavities, an homogeneous metallic film is desired to avoid the accelerating field degradation, so MoO_3 thin-films are preferred; (iii) the grain-like morphology (average grain radius ~ 50 nm), and the RMS roughness (~ 3 nm to 4 nm) is appreciably lower than that of polished polycrystalline copper (~ 7 nm), a very interesting feature to avoid the discharge since tips and roughness are thought to more easily trigger the breakdown; and (iv) hardness and reduced modulus are interestingly similar to copper to equally shield the cavity from secondary breakdowns.

Keeping the points (i)–(iv) above in mind, MoO_3 metallic thin-films (30 nm to 300 nm) deposited on copper meet a priori the requirements to mitigate trigger breakdowns which determine dark currents, with negligible impact on the accelerating field. Whether this hypothesis is confirmed, the cavity coating will allow to push E_{acc} at a fixed (low) BDR.

Nevertheless, two important issues should be tackled: (i) it is crucial to evaluate precisely how the metallic film deteriorates Q_0 for the practical application; (ii) since the transport properties are sensible to the film thickness, it is likewise important to evaluate the sensitivity of the cavity Q_0 with thickness and conductivity/resistivity of MoO_3 . With these goals, a parametric study evaluating the impact of both thickness (within the proved metallic range [16]) and resistivity of MoO_3 metallic coatings on the cavity parameters is here presented. This study is presented as the necessary continuation of the previous studies on the matter [14,15] towards the final implementation of these coatings to validate the usefulness in high-gradient accelerating structures. Formally, the analysis is equivalent

to the one presented in [17] regarding superconducting thin-films, for the limit case in which no dielectric substrate is considered between the film and the metallic cover.

The paper is organized as follows: Section 2 is dedicated to introduce the physical model for the analysis. In Section 3, the numerical results regarding the study cases are presented. In order to prove the validity of those results, an experimental section is included in Section 4. Finally, Section 5 summarizes the conclusions emphasizing the practical inferences.

2. Analysis

This section is aimed at building up a closed expression of the parameters of interest, the quality factor Q_0 and the frequency shift Δf , that completely characterize from an electromagnetic point of view the RF accelerating cavity. The electromagnetic analysis regarding the normal conducting cavity is briefly summarized, and the expression of the (bulk) surface impedance is recalled from a Perturbation Theory point-of-view [18]. Then, the effective surface impedance is obtained as the wave impedance borrowed from Transmission Line Theory [19]. In this way, the analysis of the surface impedance can be extended to the case of the cavity onto which a film is inside deposited. The computed effective surface impedance characterizes the cavity parameters as long as the perturbation remains in the same order of magnitude of that regarding the “customary” surface impedance. This is assumed as the hypothesis for each case study, to be checked a posteriori.

Electromagnetic Analysis

Accelerating beams are produced in axially symmetric RF cavities, driven with either standing (SW) or travelling waves (TW) whose fundamental mode electric field (TM₀₁₀) is oriented along the cavity axis [20]. Magnetic fields are induced in a RF regime, which leads to significant ohmic losses on the cavity normal conducting walls [21]. The quality factor Q_0 evaluates the ratio between the energy stored within the cavity and the energy dissipated through the walls in the RF period. Q_0 is constant with RF power (P_{diss}) in the linear ohmic regime but, as studied in [12], non-linear effects take part at high fields degrading it. In addition, the frequency shifting with respect to the characteristic frequency (f_0) of the “ideal” (or “unperturbed”) cavity surrounded by Perfect Electric Conductor (PEC) ($\Delta f = f - f_0$) evaluates the changes in energy (ΔU) with respect to the energy (U) stored in the PEC cavity. Q_0 and Δf are separately linked to the surface resistance (R_s) and reactance (X_s), respectively. As for the ideal cavity, $R_s = X_s = 0$, Q_0 and $\Delta f / f_0$ of the lossy cavity may be directly written as follows [20]:

$$\begin{aligned} Q_0 &= \frac{2\pi f_0 U}{P_{diss}} \equiv \frac{G}{R_s} \\ \frac{\Delta f}{f_0} &\sim \frac{\Delta U}{U} \equiv -\frac{X_s}{2G} \end{aligned} \quad (1)$$

where the factor of proportionality G is the so-called geometrical factor of the cavity. Thus, the surface impedance ($Z_s = R_s + iX_s$) completely determines the power balance in the cavity, and it ultimately defines the cavity coupling to the power source and beam and, therefore, the time response to any event (e.g., the beam loading) [20]. Consequently, it results in suitability to start the analysis of working out the expression of the effective surface impedance ($Z_{eff} = R_{eff} + iX_{eff}$) (defining the power balance) of the film, as well as the effect of having a finite impedance on accelerating the beam.

In Figure 1, both the customary (bulk) copper case (referred as bulk-Cu) and that concerning the MoO₃ thin-film deposited on bulk copper (denoted as MoO₃-film) are schematically depicted. They represent the incidence of a TM polarized wave [19] (resonant inwards) that propagates strongly attenuated within the conductors. The main difference between the bulk-Cu and the MoO₃-film lies in the thin-film allowing the impinging wave

to be reflected back from the MoO₃-Cu boundary. This feature will be proved to be useful to get $Z_{eff} \sim Z_{s,Cu}$ under certain constraints. Z_{eff} is defined as

$$Z_{eff} \equiv \frac{E|_{\partial S}}{H|_{\partial S}} = \frac{E^i|_{\partial S} + E^r|_{\partial S}}{H^i|_{\partial S} - H^r|_{\partial S}}, \tag{2}$$

symbolizing the wave impedance at the cavity surface ($n = 0$), where E^i and E^r are the impinging and reflected electric field phasors, respectively, and H^i and H^r are the respective impinging and reflected magnetic field phasors. In the case of “good” conductors ($\epsilon \ll \sigma/\omega$) in the local limit ($l \ll \delta$, l the mean free path, δ the penetration depth), and smooth surfaces ($\delta \ll 1/\chi$, χ any curvature at the boundary), those fields are TEM-like, and propagate normally to the boundary [21]. This is the case of the MoO₃-film exposed to microwaves. Thus, Equation (2) particularizes to (see Appendix A) [22]:

$$Z_{eff} = Z_{s,MoO_3} \frac{Z_{s,Cu} + iZ_{s,MoO_3} \tan(k_{MoO_3}t)}{Z_{s,MoO_3} + iZ_{s,Cu} \tan(k_{MoO_3}t)}, \tag{3}$$

where $Z_{s,MoO_3} = \sqrt{i\omega\mu_0\rho_{MoO_3}}$ and $Z_{s,Cu} = \sqrt{i\omega\mu_0\rho_{Cu}}$ are the surface impedances of (bulk) MoO₃ and Cu, respectively, $k_{MoO_3} = \sqrt{i\omega\mu_0\sigma_{MoO_3}} = (1 + i)/\delta$ is the MoO₃ (complex) wave number, and t is the MoO₃ film thickness.

Additionally, it is here recalled the effect of the finite-conducting cavity walls on the accelerating field: despite the perturbation feeds backing the electric field negatively to the accelerating field, the effect is negligible for “good” conductors. In Appendix A, the perturbation introduced in the MoO₃-film case is proved to be in the order of the bulk-Cu one as long as $Z_{eff} \sim Z_{s,Cu}$. As mentioned, this condition is checked a posteriori to be true.

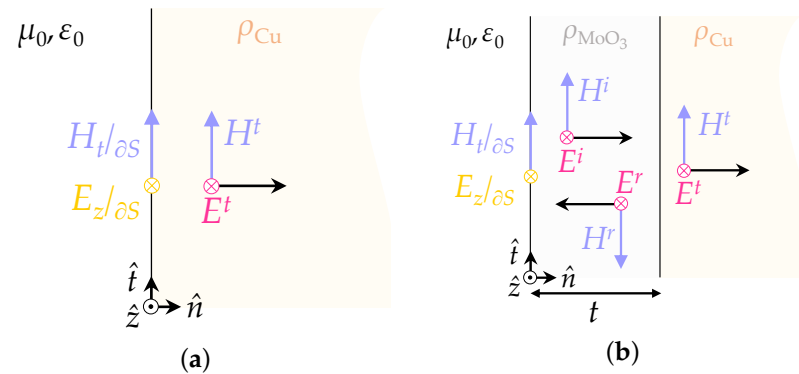


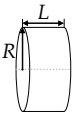
Figure 1. Simplified scheme describing the EM fields that define (a) Z_s in the bulk-Cu case and (b) Z_{eff} in the MoO₃-film case, at the cavity’s cross section boundary (∂S). In both cases, $E_z|_{\partial S}$ (plotted in yellow) represents the perturbation field (E_z in TM cases).

3. Results

The two examples to be studied, one in the X-band (as the accelerating structure used in Cryo-Cu-SLAC-#2 [5]), and the other one in the Ka-band (as that used in a Compact Light XLS [23]), reported in Table 1, are of particular interest for both experimental evaluation and future practical application. A pill-box cavity is used to compare the performance of the MoO₃-film and the bulk-Cu, taking the fundamental mode (TM₀₁₀) [20] as ($\beta = 1$) NC particle accelerator’s benchmark. This choice does not imply a loss in practicality but a useful case study for the comparison regardless of the specific final application.

Table 1. Pill-box parameters regarding the case studies. L and R are the pill-box length and radius.

Case Study	f_0 [GHz]	G [Ω]	L [mm]	R [mm]
X-band (Cryo-Cu-SLAC-#2) [5]	11.4294	256.77	13.12	10.04
Ka-band (Compact Light XLS) [23]	36.0	256.77	4.164	3.188



The cavity linear response is fully captured in Q_0 and Δf , redefined using R_{eff} and X_{eff} in place of R_s and X_s in Equation (1), respectively. In Figure 2, Q_0 and $\Delta f/f_0$ concerning the case study in the X-band are represented as a function of the MoO₃ layer thickness, both parametrized by ρ_{MoO_3}/ρ_{Cu} (with $\rho_{Cu} = 1.67 \mu\Omega\text{ cm}$), whereas in Figure 3 the respective functions for the case study in the Ka-band are plotted.

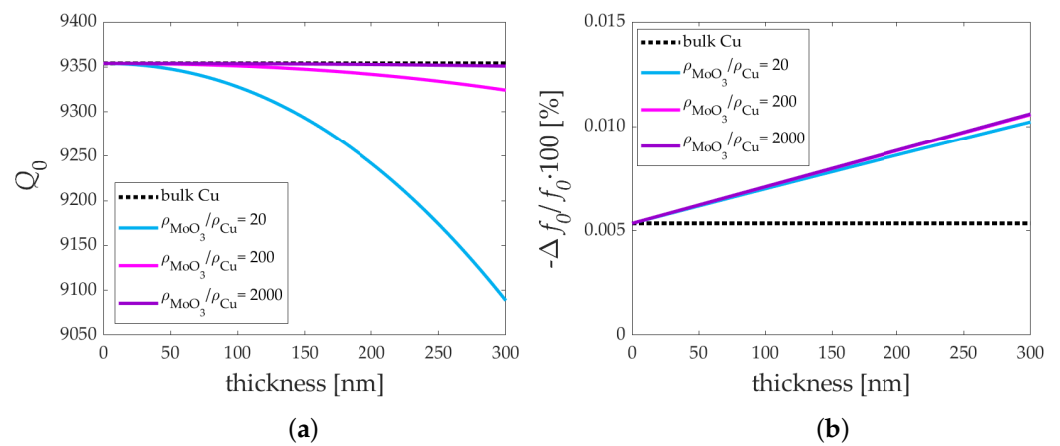


Figure 2. Pill-box parameters at $f_0 \approx 11.4$ GHz: Q_0 (a) and $-\Delta f/f_0$ (b), as a function of MoO₃ film thickness and parameterized by the ratio between the coating and substrate resistivities (ρ_{MoO_3}/ρ_{Cu}).

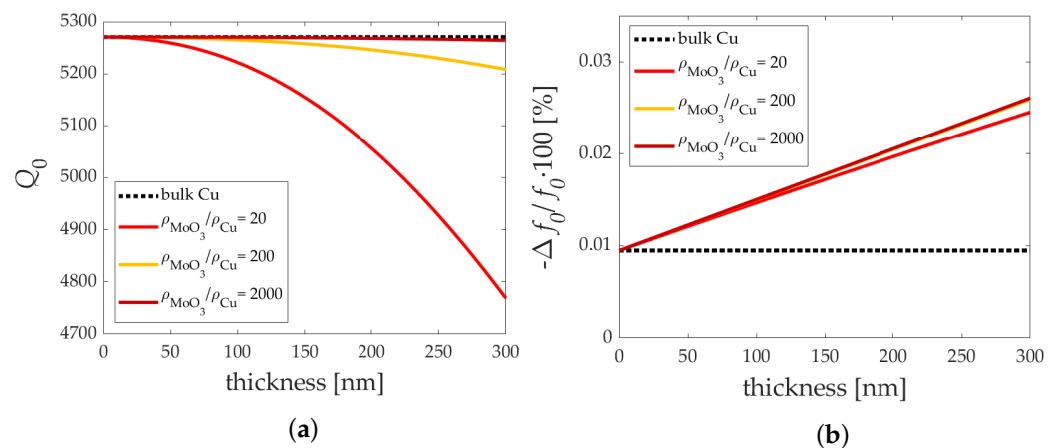


Figure 3. Pill-box parameters at $f_0 = 36.0$ GHz: Q_0 (a) and $-\Delta f/f_0$ (b), as a function of MoO₃ film thickness and parameterized by the ratio between the coating and substrate resistivities (ρ_{MoO_3}/ρ_{Cu}).

From the results shown in Figures 2 and 3, the first important result of the study emerges: both Q_0 and Δf of the film-layered cavity essentially behave as in the bulk case when the coating consists of a thin-film, as shown experimentally in Section 4. At the smallest thicknesses, $Q_0 \propto f^{-\frac{1}{2}}$ and $\Delta f \propto f^{\frac{1}{2}}$, as bulk-Cu. However, perhaps counter-intuitively, the extra losses caused by the deposited film are slightly larger when the resistivity of finite-thickness conductive MoO₃ is closer to that of copper, while this effect does not appear when comparing Δf . As a consequence, for a fixed thickness, a minimum

Q_0 is reached at a finite layer conductivity, as shown in Figure 4. These observations can be explained by the fact that the film becomes electrically thinner at lower frequencies or greater resistivity. This latter feature also favors the mismatch at the film-substrate boundary so that impinging and reflected waves tend to cancel out each other. On the contrary, as the coating becomes thicker, Q_0 naturally degrades and Δf increases, as shown in Figure 5 for the $f_0 \approx 11.4$ GHz case (in general, the quality factor degradation and frequency shifting are more noticeable at a higher frequency). As expected, in the bulk case the curves tend to saturate close to the bulk copper case as $\rho_{\text{MoO}_3}/\rho_{\text{Cu}} \rightarrow 1$. Notice that the Q_0 curves intersect due to the opposite arrangement in the thin-film and bulk cases. This occurs because highly resistive metal coatings in the thin-film regime yields the copper performance with good approximation.

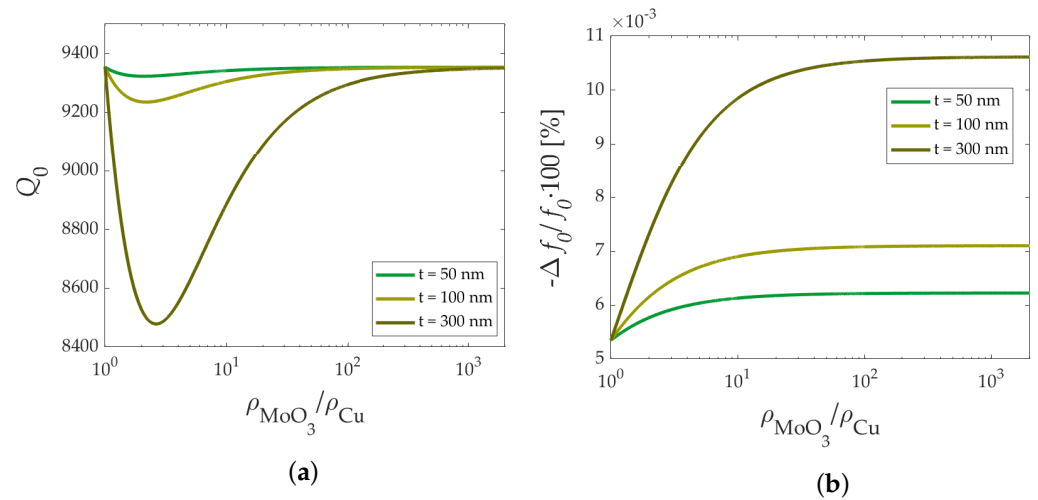


Figure 4. Pill-box parameters at $f_0 \approx 11.4$ GHz: (a) Q_0 and (b) $-\Delta f/f_0$, as a function of the ratio between the coating and substrate resistivities ($\rho_{\text{MoO}_3}/\rho_{\text{Cu}}$), and parameterized by the MoO_3 film thickness.

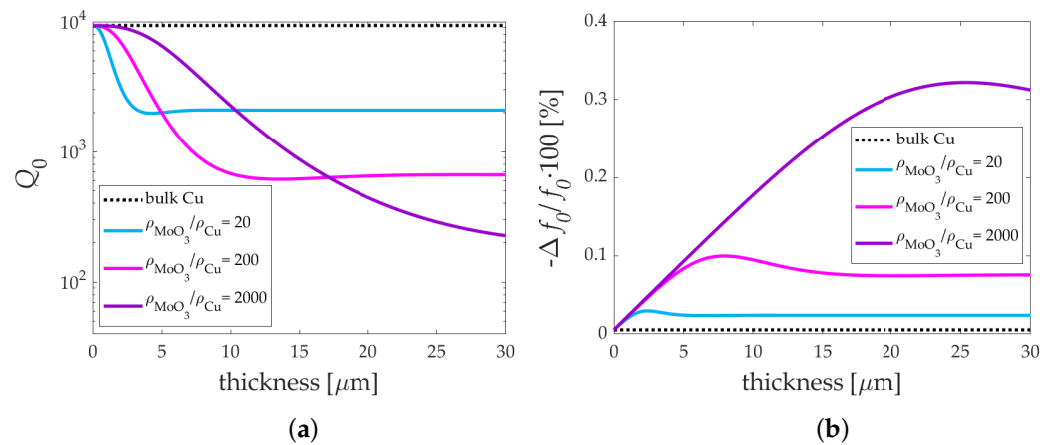


Figure 5. Pill-box parameters at $f_0 \approx 11.4$ GHz: (a) Q_0 and (b) $-\Delta f/f_0$, as a function of MoO_3 film thickness in the bulk scale, and parameterized by the ratio between the coating and substrate resistivities ($\rho_{\text{MoO}_3}/\rho_{\text{Cu}}$).

Additionally, as a second important result of this work, it is worth stressing that both Q_0 and Δf are not very sensitive to film properties, in terms of resistivity (defined as $\partial Q_0/\partial \rho_{\text{MoO}_3}$ and $\partial \Delta f/\partial \rho_{\text{MoO}_3}$; those derivatives are minor with respect to Q_0 and Δf , respectively) and thickness (defined as $\partial Q_0/\partial t$ and $\partial \Delta f/\partial t$; those derivatives are minor with respect to Q_0 and Δf , respectively). The Q_0 sensitivity decreases as the film is electrically thinner, whereas Δf sensitivity is constant with film thickness and remains practically unchanged with frequency and MoO_3 resistivity (these features can be appreciated directly

in Figures 2 and 4 at the lowest thicknesses and largest resistivity ratios, respectively). This means that the cavity behavior would not be impacted by even relatively large inhomogeneities of the coating properties.

Finally, the validity of the model used throughout the analysis is checked in Figure 6. As the modulus of the effective impedance of the MoO₃-film is in the same order of the one regarding the bulk-Cu surface impedance, it may be safely said that the perturbation is upon the same order at both frequency bands. As the bulk-Cu is well described by means of the first-order perturbation, the same holds for the layered structure with the MoO₃-film.

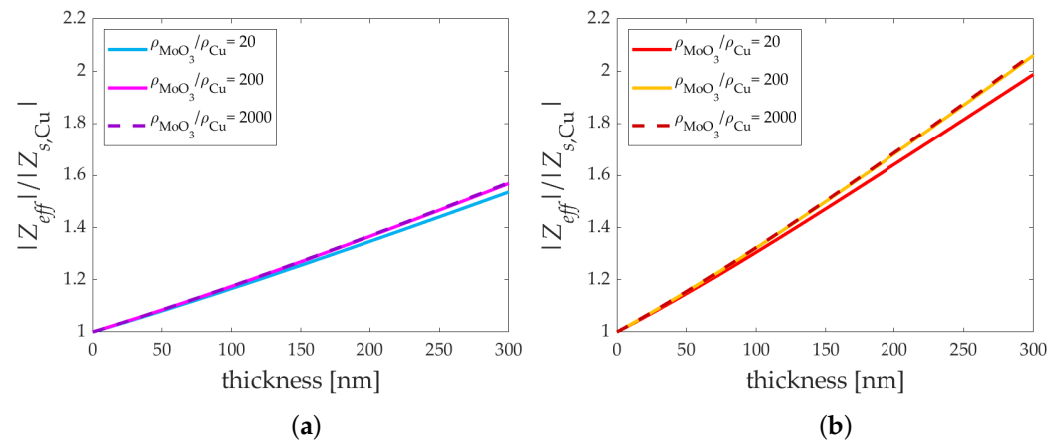


Figure 6. Ratio $|Z_{eff}|/|Z_{s,Cu}|$ that establishes the validity of the first-order perturbation ($\epsilon \rightarrow 0$) at (a) $f_0 \approx 11.4$ GHz and (b) $f_0 = 36.0$ GHz.

4. Experimental Section

This section is intended to provide an experimental validation on the negligible influence of Mo oxide thin-films deposited on copper upon the cavity quality factor. It does not constitute, however, a demonstration of the full validity of the model, but a particular output in agreement with the results presented in Section 3. On the other hand, while the complete description of the measurement method, apparatus characteristics, and performances are thoroughly described in [24,25], here just the most significant aspects of the measurement procedure and the obtained results regarding the effective surface resistance (R_{eff}) of Mo thin-films are reported to support the potential use in accelerating cavities. As the goal of this measurement is to demonstrate that the R_{eff} of Mo oxide thin-film is indistinguishable from the R_s of Cu, differential measurements (ΔR_s) are carried out rather than the absolute ones, also in view of the reduced measurement uncertainty this non-calibrated method entails.

A Hakki–Coleman sapphire-loaded resonator equipped with an upper open window from which the sample under test is exposed to the excited mode (TE₀₁₁) is used, connected to an Anritsu 37269D Vector Network Analyzer (VNA). The employed resonator facilitates the sample mounting, so that the measurement repeatability is optimized. The measured samples are of ~ 1 cm² of bulk copper (used as reference), and ~ 50 nm and ~ 100 nm of Mo oxide layers deposited on copper. Each sample is mounted $n = 11$ times. For each mounting, the transmission scattering parameters (measured at ~ 5 the full-width half-maximum (FWHM) of the resonance centered at $f_0 \approx 12.976$ GHz, and sampling the frequency span with the maximum number of points (1601) available) are fitted by means of a Lorentzian curve, as shown in Figure 7, and described in [24] in detail. The fitting parameter under investigation is the loaded quality factor Q_L , which essentially comprises the losses of each component of the resonator (since the port coupling is negligible in comparison with the resonator Q_0), including the sample under test.

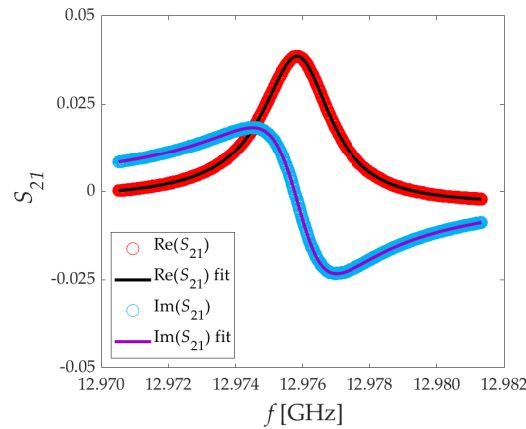


Figure 7. Resonance of the transmission scattering parameter S_{21} . The measurements are fitted by means of a Lorentzian curve, as described in [24].

The mean Q_L (\bar{Q}_L) together with the measurement standard deviation (σ_{Q_L}) and the mean value uncertainty ($u(\bar{Q}_L)$) are reported in Table 2. From these results, it can be seen that (i) as \bar{Q}_L of the mounting with the bulk and that of the 100 nm Mo oxide coating are the same, it is already evident that those samples are indistinguishable in terms of R_s ; and (ii) both the relatively low statistical deviation and measurement uncertainty point to the high repeatability and trueness of the experiment, respectively. Furthermore, and based on the high repeatability of the mounting, the differential measurements (with respect to copper) may be obtained once the sample geometrical factor ($G_s \approx 3380 \Omega$) is computed. Those are also shown in Table 2. As seen through the obtained results, the differences on R_s between the Mo oxide films and bulk Cu are below the measurement uncertainty (which is in the order $\sim 1 \text{ m}\Omega$, as stated in [24]), and so the potential Q_0 of the coated accelerating cavity would be close to the bulk one. Reciprocally, the minimum $\rho_{\text{MoOx},\text{min}}$ that fits the $u(\Delta R)$ in our model is reported in Table 2 (for 50 nm and 100 nm, taking $\rho_{\text{Cu}} = 1.67 \mu\Omega \text{ cm}$, as for the numerical analysis presented in Section 3). As the true resistivity of the film is expected to be always greater than those estimated minimums, the introduced model is further proved to be valid.

Table 2. Summary of the measurement parameters and the corresponding uncertainties regarding Cu bulk and Mo thin-film samples. For the differential measurement, the Cu samples is used as reference.

Sample	\bar{Q}_L	σ_{Q_L}	$u(\bar{Q}_L)$	ΔR [mΩ]	$u(\Delta R)$ [mΩ]	$\rho_{\text{MoOx},\text{min}}$ [μΩcm]
Bulk Cu	5178	13	9	-	-	-
50 nm MoOx-on-Cu	5172	5	3	-0.7	1.2	1.74
100 nm MoOx-on-Cu	5178	12	8	0	1.5	1.76

5. Conclusions

In this paper, the effects of MoO₃ coatings on the accelerating cavity parameters completely determining their linear RF response Q_0 and $\Delta f/f$ have been thoroughly studied. For this purpose, the classical expression describing the Z_s of bulk conductors has been generalized to the case of normal conducting thin-film deposited on a metallic substrate. At the same time, the perturbation on the accelerating field introduced by the coating finite conductivity was rigorously evaluated. Then, Z_{eff} has been numerically checked for a couple of case studies at different frequency bands. In addition, experimental results are provided proving the negligible impact of Mo oxide coatings deposited on Cu in terms of R_s , a result which is explained by this numerical analysis and the underlying model.

The computed results show (i) relatively little impact of (30 to 300) nm MoO₃ metallic coatings on both Q_0 and Δf , and the magnitude of the accelerating cavity field, since $Z_{\text{eff}} \sim Z_{s,\text{Cu}}$ at various microwave frequencies. In addition, (ii) the coated cavity performs

almost sensitive to thickness and resistivity variations within large ranges, making the cavity performance highly robust against coating inhomogeneities. As the negligible impact on the cavity parameters is a pre-condition for the subsequent coating deposition work, these results allow for MoO₃ as potential candidate to mitigate the BDR with origin in dark currents due to its intrinsically high WF.

As the analysis has been treated in a generalized way, and the respective parametrizations have been explored in a relatively large range, one can safely extrapolate these results to either molybdenum coatings made of different phases (e.g., molybdenum dioxide MoO₂, or heterogeneous molybdenum metallic films [26]) or other conductive materials.

Author Contributions: Conceptualization, S.S. and B.S.; formal analysis, P.V.G. and N.P.; manuscript preparation, P.V.G. and N.P.; critical reading, S.S., M.C., L.G., A.M., B.S., A.A., K.T. and E.S.; supervision, S.S., B.S. and N.P.; funding acquisition, E.S. and N.P. All authors have read and agreed to the published version of the manuscript.

Funding: This research received no external funding.

Data Availability Statement: Data are provided in the figures and tables of the article. Data files are available upon request to the corresponding author.

Conflicts of Interest: The authors declare no conflict of interest.

Appendix A

The EM analysis regarding the modes of the accelerating cavity (TM modes) surrounded by film is tackled here. The “successive approximation scheme” (i.e., the perturbation analysis) presented in [21] for the bulk conductor is extended to the case in which the penetrating field is reflected at the film–substrate boundary (see Figure 1). The asymptotic expression of the field is thus obtained.

The accelerating field (E_z) completely determines the EM fields of TM modes in the ideal cavity. At each cavity cross-section (see Figure A1), $\Phi_0 \equiv E_z$ denotes the exact solution of the corresponding Dirichlet-2D-BVP:

$$\nabla^2 \Phi_0 + \gamma^2 \Phi_0 = 0 \quad (\Phi_0 = 0 \text{ on } \partial S); \tag{A1}$$

where $\gamma^2 = (\omega/c)^2 - k_z^2$ and k_z is the wave number along the perpendicular direction (e.g., $k_z = \pm p\pi/L$ in cylindrical z -invariant coordinate systems, being L the cavity’s length).

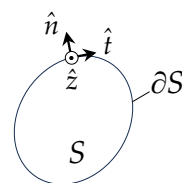


Figure A1. Cross-section defining the BPV. The field penetrates normally to the contour (∂S), along which the EM field is continuous. The wave number k_z ultimately defines the mode spectrum.

The sought solution is hypothesized to be asymptotically equal to

$$\Phi \sim \Phi_0 + \epsilon \Phi_1 \quad (\epsilon \rightarrow 0), \tag{A2}$$

where Φ_1 is the first-order correction. Φ_1 can be computed as a function of Φ_0 by imposing the continuity of the magnetic field at the boundary (see the notation used in Figure 1):

$$H_t|_{\partial S} \equiv i \frac{\hat{z} \times \nabla_t \Phi_0|_{\partial S}}{\omega \mu_0} \left[\frac{1}{1 - k_z^2 (\frac{c}{\omega})^2} \right] = H|_{\partial S} \equiv H^i|_{\partial S} (1 - \Gamma_{eff}), \text{ with} \tag{A3}$$

$$\Gamma_{eff} = \frac{Z_{eff} - Z_{s,MoO_3}}{Z_{eff} + Z_{s,MoO_3}} \tag{A4}$$

the effective reflection coefficient at the boundary cavity-film. Furthermore, the incident field (E^i) is obtained by means of the characteristic impedance (i.e., the surface impedance), which points to $-\hat{z}$. Further continuity of the electric field leads to negative feedback to be added as perturbation to the accelerating field:

$$\epsilon\Phi_1|_{\partial S} \equiv -E^i|_{\partial S} (1 + \Gamma_{eff}) = -Z_{s,MoO_3} H^i|_{\partial S} (1 + \Gamma_{eff}). \quad (A5)$$

By solving $H^i|_{\partial S}$ from Equation (A3) and substituting it in Equation (A5), and further using Γ_{eff} from Equation (A4), $\epsilon\Phi_1$ may be rewritten as:

$$\epsilon\Phi_1|_{\partial S} = -iZ_{eff} \frac{(\hat{n} \cdot \nabla\Phi_0)|_{\partial S}}{\omega\mu_0} \left[\frac{1}{1 - k_z^2 \left(\frac{c}{\omega}\right)^2} \right]. \quad (A6)$$

In Equation (A6), the term Z_{eff} ultimately controls the definitive validity of Equation (A2).

In order to obtain Z_{eff} , Γ_{eff} is written as the transformation of the reflection coefficient [19] at the boundary film-substrate (Γ_b):

$$\begin{aligned} \Gamma_{eff} &= \Gamma_b e^{-2ik_{MoO_3}t}, \text{ with} \\ \Gamma_b &= \frac{Z_{s,Cu} - Z_{s,MoO_3}}{Z_{s,Cu} + Z_{s,MoO_3}}. \end{aligned} \quad (A7)$$

Then, Z_{eff} is solved by substituting Equation (A7) in Equation (A4), leading to the expression in Equation (3) used for the analysis.

References

1. Sicking, E.; Ström, R. From precision physics to the energy frontier with the Compact Linear Collider. *Nat. Phys.* **2020**, *16*, 386–392. [CrossRef]
2. Emma, P.; Akre, R.; Arthur, J.; Bionta, R.; Bostedt, C.; Bozek, J.; Brachmann, A.; Bucksbaum, P.; Coffee, R.; Decker, F.J.; et al. First lasing and operation of an ångstrom-wavelength free-electron laser. *Nat. Photon.* **2010**, *4*, 641–647. [CrossRef]
3. Lindroth, E.; Calegari, F.; Young, L.; Harm, M.; Dudovich, N.; Berrah, N.; Smirnova, O. Challenges and opportunities in attosecond and XFEL science. *Nat. Rev. Phys.* **2019**, *1*, 107–111. [CrossRef]
4. Wang, F.; Adolphsen, C.; Nantista, C. Performance limiting effects in X-band accelerators. *Phys. Rev. ST Accel. Beams* **2011**, *14*, 010401. [CrossRef]
5. Cahill, A.D.; Rosenzweig, J.B.; Tantawi, S.G.; Weathersby, S. High gradient experiments with X-band cryogenic copper accelerating cavities. *Phys. Rev. Accel. Beams* **2018**, *21*, 102002. [CrossRef]
6. Grudiev, A.; Calatroni, S.; Wuensch, W. New local field quantity describing the high gradient limit of accelerating structures. *Phys. Rev. ST Accel. Beams* **2009**, *12*, 102001. [CrossRef]
7. Wuensch, W. High-Gradient Breakdown in Normal-Conducting RF cavities. In Proceedings of the 8th European Particle Accelerator Conference, Paris, France, 3–7 June 2002; p. 134.
8. Nordlund, K.; Djurabekova, F. Defect model for the dependence of breakdown rate on external electric fields. *Phys. Rev. ST Accel. Beams* **2012**, *15*, 071002. [CrossRef]
9. Rosenzweig, J.B.; Cahill, A.; Dolgashev, V.; Emma, C.; Fukasawa, A.; Li, R.; Limborg, C.; Maxson, J.; Musumeci, P.; Nause, A.; et al. Next generation high brightness electron beams from ultrahigh field cryogenic rf photocathode sources. *Phys. Rev. Accel. Beams* **2019**, *22*, 023403. [CrossRef]
10. Wuensch, W.; Achard, C.; Dobert, S.; Braun, H.H.; Syratcev, I.; Taborelli, M.; Wilson, I. Demonstration of high-gradient acceleration. In Proceedings of the 2003 Particle Accelerator Conference, Portland, OR, USA, 12–16 May 2003; Volume 1, pp. 495–497. [CrossRef]
11. Wuensch, W.; Grudiev, A.; Heikkinen, S.; Syratcev, I.; Taborelli, M.; Wilson, I.; Adolphsen, C.; Döbert, S. A High-Power Test of an X-Band Molybdenum-Iris Structure. In Proceedings of the 22nd International Linear Accelerator Conference, Lübeck, Germany, 16–20 August 2004. Available online: <https://cds.cern.ch/record/790355> (accessed on 19 October 2023).
12. Cahill, A.D.; Rosenzweig, V.A.; Dolgashev, V.A.; Li, Z.; Tantawi, S.G.; Weathersby, S. rf losses in high gradient cryogenic copper cavity. *Phys. Rev. Accel. Beams* **2018**, *21*, 061301. [CrossRef]
13. Fowler, R.H.; Nordheim, L. Electron Emission in Intense Electric Fields. *Proc. R. Soc. Lond.* **1928**, *119*, 173–181. Available online: <https://www.jstor.org/stable/95023> (accessed on 29 July 2023).
14. Bini, S.; Spataro, B.; Marcelli, A.; Sarti, S.; Dolgashev, V.A.; Tantawi, S.; Yeremian, A.D.; Higashi, Y.; Grimaldi, M.G.; Romano, L.; et al. Molybdenum sputtering film characterization for high gradient accelerating structures. *Chin. Phys. C* **2013**, *37*, 097005. [CrossRef]

15. Scifo, J.; Marcelli, A.; Spataro, B.; Hampai, D.; Dabagov, S.; Sarti, S.; Di Trolio, A.; Moscatelli, R.; Macis, S.; Faillace, L. Molybdenum Oxides Coatings for High Demanding Accelerator Components. *Instruments* **2019**, *3*, 61. [[CrossRef](#)]
16. Macis, S.; Aramo, C.; Bonavolontà, C.; Cibin, G.; D'Elia, A.; Davoli, I.; De Lucia, M.; Lucci, M.; Lupi, S.; Miliucci, M.; et al. MoO₃ films grown on polycrystalline Cu: Morphological, structural, and electronic properties. *J. Vac. Sci. Technol. A* **2019**, *37*, 021513. [[CrossRef](#)]
17. Klein, N.; Chaloupka, H.; Mueller, G.; Orbach, S.; Piel, H.; Roas, B.; Schultz, L.; Klein, U.; Peiniger, M. The effective microwave surface impedance of high- T_c thin-films. *J. Appl Phys.* **1990**, *67*, 6940. [[CrossRef](#)]
18. Erdélyi, A. *Asymptotic Expansions*; Dover Publications, Inc.: New York, NY, USA, 1956.
19. Balanis, C.A. *Advanced Engineering Electromagnetics*, 1st ed.; John Wiley & Sons, Inc.: New York, NY, USA, 1989.
20. Rosenzweig, J.B. *Fundamentals of Beam Physics*, online ed.; Oxford Academic: Oxford, UK, 2003. [[CrossRef](#)]
21. Jackson, J.D. *Classical Electrodynamics*, 3rd ed.; John Wiley & Sons, Inc.: New York, NY, USA, 1999.
22. Pompeo, N.; Torokhtii, K.; Silva, E. Surface impedance measurements in thin conducting films: Substrate and finite-thickness-induced uncertainties. In Proceedings of the IEEE International Instrumentation and Measurement Technology Conference (I2MTC), Turin, Italy, 22–25 May 2017; pp. 1–5. [[CrossRef](#)]
23. Spataro, B.; Behtouei, M.; Di Paolo, F.; Leggieri, A. A low-perveance electron gun for a high-efficiency Ka-band klystron. *Eur. Phys. J. Plus* **2022**, *137*, 769. [[CrossRef](#)]
24. Alimenti, A.; Torokhtii, K.; Vidal García, P.; Pompeo, N.; Silva, E. Design and Test of a New Dielectric-Loaded Resonator for the Accurate Characterization of Conductive and Dielectric Materials. *Sensors* **2023**, *23*, 518. [[CrossRef](#)] [[PubMed](#)]
25. Alimenti, A.; Pittella, E.; Torokhtii, K.; Pompeo, N.; Piuze, E.; Silva, E. A Dielectric Loaded Resonator for the Measurement of the Complex Permittivity of Dielectric Substrates. *IEEE Trans. Instrum. Meas.* **2023**, *72*, 6001009. [[CrossRef](#)]
26. Marcelli, A.; Spataro, B.; Castorina, G.; Xu, W.; Sarti, S.; Monforte, F.; Cibin, G. Materials and Breakdown Phenomena: Heterogeneous Molybdenum Metallic Films. *Condens. Matter* **2017**, *2*, 18. [[CrossRef](#)]

Disclaimer/Publisher's Note: The statements, opinions and data contained in all publications are solely those of the individual author(s) and contributor(s) and not of MDPI and/or the editor(s). MDPI and/or the editor(s) disclaim responsibility for any injury to people or property resulting from any ideas, methods, instructions or products referred to in the content.